Stochastic model for earthquake ground motion using wavelet packets

Y. Yamamoto & J. W. Baker
Department of Civil & Environmental Engineering
Stanford University, CA 94305, U.S.A.

ABSTRACT: For performance-based design, non-linear dynamic structural analysis for various types of input ground motions is required. Stochastic (simulated) ground motions are sometimes useful as input motions, because unlike recorded motions they are not limited in number and because their properties can be varied systematically to understand the impact of ground motion properties on structural response. Here a stochastic ground motion model with time and frequency nonstationarity is developed using wavelet packets. Wavelet transform is a tool for analyzing time-series data with time and frequency nonstationarity, as well as simulating such data. Wavelet packet transform is an operation that decomposes time-series data into wavelet packets in the time and frequency domain, and its inverse transform reconstructs a time-series from wavelet packets. The characteristics of a nonstationary ground motion therefore can be modeled intuitively by specifying the amplitudes of wavelet packets at each time and frequency. In the proposed model, 13 parameters are sufficient to completely describe the time and frequency characteristics of a ground motion. These parameters can be computed from a specific target ground motion recording or by regression analysis based on a large database of recordings. The simulated ground motions produced by the proposed model reasonably match the target ground motion recordings in several respects including the spectral acceleration, inelastic response spectra, duration, bandwidth, and time and frequency nonstationarity. In addition, the median and logarithmic standard deviation of the spectral acceleration of the simulated ground motions match those of the published empirical ground motion prediction. These results suggest that the synthetic ground motions generated by the proposed model can be used for the non-linear dynamic structural analysis as the input ground motions.

1 INTRODUCTION

1.1 *Background*

Performance-based design generally requires the use of large numbers of input ground motions for non-linear dynamic structural analysis, but the number of available recorded ground motions is limited and may not be sufficient for characterizing a particular analysis condition. In order to obtain enough numbers of the ground motions, ground motion scaling and spectral matching are widely used to adjust recorded ground motions and make them more representative of particular analysis conditions. However since the scaling and the spectrum matching modify the characteristics of the ground motion recordings, they are not consistent with the physical conditions and the results from these operations could have the characteristics different from those of the actual recordings (Luco and Bazzurro 2007, Bazzuro and Luco 2006). Therefore the artificial earthquake ground motions that are consistent with both the physical condition and the characteristics of the actual ground motion recordings are needed.

There are three general classes of strong ground motion simulation techniques: physics-based models and stochastic models. Physics-models simulate ground motions by modeling the fault rupture, the resulting wave propagation, and the near-surface site amplification. Since they require precise information about the earthquake source, wave propagation path, and soil structure, it is difficult and computationally expensive to produce simulations that cover the range of possible future earthquakes. The problem is especially difficult to simulate high-frequency motions.

Stochastic models, in contrast, are empirically calibrated approaches that directly simulate the ground motion instead of modeling fault rupture, wave propagation, and site amplification. This approach is in general computationally inexpensive, and is equally applicable for high and low frequencies. However since most stochastic models are based on modified Gaussian white noise processes, it is difficult to simulate the time and frequency nonstationarity.

Hybrid method (e.g., Graves and Pitarka 2010) combines two or more models. Typically it combines

the physics-based models for low frequency components and stochastic models for high frequency components through frequency filters.

For stochastic ground motion models, modeling of the temporal and spectral nonstationarities is important because the earthquake response of non-linear structures is affected by these nonstationarities of strong ground motions (e.g. Chakravorty and Vanmarck 1973 and Spanos et al. 2007). The temporal nonstationarity is defined as change in the amplitude of the ground motion with time, and the spectral nonstationarity is defined as change in the frequency content of the ground motion with time.

Tho common types of stochastic ground motion models are (stationary or nonstationary) Gaussian white-noise processes, and the evolutionary power spectral density (EPSD) models. Using the first type of model, Rezaeian and Kiureghian(2008, 2010) developed a fully nonstationary stochastic model which uses a modulated filtered white-noise process in the time domain. Their model has the advantage that the temporal and spectral nonstationarities are separately computed by modulating the response of a linear filter having time-varying characteristics with a white-noise excitation. On the other hand, Spanos and Failla (2004) proposed a wavelets-based method to estimate the EPSD of the target ground acceleration record. They used the continuous wavelet transform (CWT) instead of the short-time Fourier transform (STFT) in order to achieve an enhanced time resolution for high frequency components. Their implementation was limited, however, to producing simulations that reproduced properties of a "seed" ground motion that was used for calibration, rather than producing simulations for an arbitrary future earthquake scenario.

The model proposed here is based on Thráinsson and Kiremidjian (2002) and we extend their model using wavelet packet transform (WPT) since it can fully control the time and frequency characteristic of time series. The WPT is employed to approximate the EPSD for stochastic ground motion modeling. The WPT is the extended version of the discrete wavelet transform (DWT), and it has the advantages of being able to control amplitudes in the time and frequency domain with constant resolution and of allowing reconstruction of the original time series from the wavelet packets. By using WPT, one can thus maintain temporal and spectral nonstationarities in the time and frequency domain.

Since wavelet packets of actual signals tend to be sparse, our model simulates ground motions by producing two groups of wavelet packets. The major group, which contributes 70% of the energy of the generated ground motion, consists of wavelet packets with a bivariate lognormal distribution for their time and frequency locations and an independent exponential distribution for their amplitudes. The minor group of coefficients, which contributes the remaining energy, have a bivariate lognormal distribution as a

time and frequency modulating function. Further details are given below. 13 parameters are required to fully specify the model, and predictive equations for these parameters (as a function of earthquake magnitude, distance and site conditions) are calibrated using regression analysis on a large database of recorded ground motions each of which has had these 13 parameters computed.

The proposed model has the following advantages: a) the temporal and the spectral nonstationarity can be controlled by adjusting the parameters describing amplitudes of wavelet packets, b) the model is empirically calibrated and produces motions that are consistent in their important characteristics with observed ground motion recordings and ground motion prediction models, and c) the procedure is computationally inexpensive, so we can obtain large numbers of ground motions.

1.2 *Wavelet packet transform and EPSD*

Several approaches are available to capture time and frequency nonstationarity, such as group delay time, instantaneous frequency, and zero-crossing rate. However nonstationarity can be expressed in only one of the time or frequency axis using those tools, so it is difficult to characterize the whole distribution of time and frequency characteristics. Short-Time Fourier Transform (STFT) can detect time and frequency characteristics in the time and frequency domain, but it is difficult to reconstruct a time series using an inverse of the STFT.

Here we employ the wavelet packet transform for modeling time series with the time and frequency nonstationarity because it can decompose the time series into the wavelet packets in the time and frequency domain and it can reconstruct the time series from the wavelet packets.

The forward and inverse wavelet packet transform are defined as follows:

$$c_{j,k}^i = \int_{-\infty}^{\infty} x(t) \psi_{j,k}^i(t) dt \tag{1}$$

$$x(t) = \sum_{i=1}^{2^j} \sum_{k=1}^{2^{N-j}} c_{j,k}^i \psi_{j,k}^i(t) \tag{2}$$

where $x(t)$ is the time series, 2^N is the number of data in the time series, $c_{j,k}^i$ denotes the ith set of wavelet packets at the jth scale parameter and k is the translation parameter, and $\psi_{j,k}^i(t)$ is the wavelet packet function, which is localized around the central time t_k and frequency f_i. In our model, the wavelet packet function is computed from finite impulse response based approximation of the Meyer wavelet (Meyer 1986) because of its orthogonality and localization property.

The evolutionary power spectral density (EPSD) can be estimated using continuous wavelet transform

(Spanos and Failla 2004). Here we approximate the EPSD using the wavelet packets. An arbitrary non-stationary process described by the following general form (Priestley 1996)

$$x(t) = \int_{-\infty}^{\infty} A(\omega,t)e^{i\omega t}d\bar{Z}(\omega) \qquad (3)$$

where $A(\omega,t)$ is the time- and frequency-dependent modulating function, and $\bar{Z}(\omega)$ is a complex random process with orthogonal increments such that

$$E[d\bar{Z}(\omega)d\bar{Z}^*(\omega)'] = \begin{cases} S_{\overline{ff}}(\omega)d\omega & \omega = \omega' \\ 0 & \text{otherwise} \end{cases} \qquad (4)$$

where $E[\cdot]$ indicates a expectation and $S_{\overline{ff}}(\omega)$ is the two-sided power spectral density (PSD) for the zero mean stationary process as follows:

$$\bar{x}(t) = \int_{-\infty}^{\infty} e^{i\omega t}d\bar{Z}(\omega) \qquad (5)$$

The two-sided EPSD of $x(t)$ is then defined as

$$S_{ff}(\omega,t) = |A(\omega,t)|^2 S_{\overline{ff}}(\omega) \qquad (6)$$

The wavelet packets of the process $x(t)$ at a scale i and a position k can then be computed as

$$c_{j,k}^i = \int_{-\infty}^{\infty}\left\{\int_{-\infty}^{\infty} A(\omega,t)e^{i\omega t}d\bar{Z}(\omega)\right\}\psi_{j,k}^i(t)dt \qquad (7)$$

Due to the time localization properties of the wavelet $\psi_{j,k}^i(t)$ around the time t_k, it can be assumed that

$$c_{j,k}^i \approx \int_{-\infty}^{\infty} A(\omega,t_k)e^{i\omega t_k}\Psi_j^i(\omega)d\bar{Z}(\omega) \qquad (8)$$

where $\tau = t - t_k$ and $\Psi_j^i(\omega)d\bar{Z}(\omega)$ is a complex random process, which has the orthogonality property of $\bar{Z}(\omega)$. Therefore, it supports the statement that the wavelet packets at scale i, $c_{j,k}^i$ can be considered a nonstationary oscillatory process with respect to the time t_k. Then, the two-sided EPSD of $x(t)$ is given by

$$S_{WW}^{c_{j,k}^i} = |A(\omega,t)|^2|\Psi_j^i(\omega)|^2 S_{\overline{ff}}(\omega) \qquad (9)$$

Further, an expectation of squared $c_{j,k}^i$ can be defined by the equation

$$E[|c_{j,k}^i|^2] = \int_{\infty}^{\infty} S_{WW}^{c_{j,k}^i}d\omega \qquad (10)$$

$$\approx \int_{\infty}^{\infty} |A(\omega,t)|^2|\Psi_j^i(\omega)|^2 S_{\overline{ff}}(\omega)d\omega \qquad (11)$$

since $\Psi_j^i(\omega)$ is localized around ω_i.

Therefore $E[|c_{j,k}^i|^2]$ can be considered to be an approximation of the EPSD, and we can generate the time-series data with particular time and frequency characteristics using the wavelet packets and we can generate the time series with particular time and frequency characteristics using the wavelet packets. Figure 1 shows the relationship between the time, frequency, and the wavelet domain.
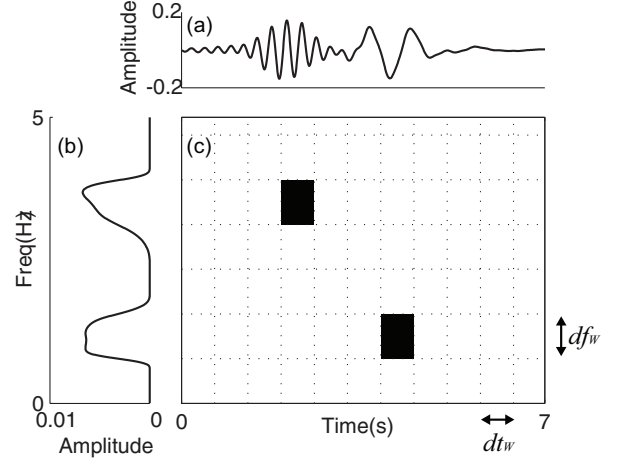

Figure 1: The relationship between the time, frequency, and wavelet domain. (a) time series, (b) Fourier spectrum, and (c) wavelet packets.

1.3 Relationship between time history, Fourier spectrum, and wavelet packets

In order to control the time and frequency characteristics of the acceleration time series, we employ the following five parameters:

$$E_{acc} = \int_{-\infty}^{\infty} |x(t)|^2 dt = \sum_i\sum_k |c_{j,k}^i|^2 \qquad (12)$$

$$E_{th}(t) = \int_{-\infty}^{\infty} t\,|x(t)|^2 dt/E_{acc} \qquad (13)$$

$$\frac{\int_{t_5}^{t_5+t_{95-5}} |x(t)|^2 dt}{E_{acc}} = 0.9,\ \frac{\int_0^{t_5} |x(t)|^2 dt}{E_{acc}} = 0.05 \qquad (14)$$

$$E_{th}(f) = \int_{-\infty}^{\infty} f\,|\hat{x}(f)|^2 df/E_{acc} \qquad (15)$$

$$\frac{\int_{f_5}^{f_5+f_{95-5}} |\hat{x}(f)|^2 df}{E_{acc}} = 0.9,\ \frac{\int_0^{f_5} |\hat{x}(f)|^2 df}{E_{acc}} = 0.05 \qquad (16)$$

where E_{acc} is the total energy of the acceleration time series, $E_{th}(t)$ is the temporal centroid, t_{95-5} is the $5-95\%$ significant duration (Trifunac and Brady 1975) that contains 90% of the total energy, $E_{th}(f)$ is the spectral centroid, and f_{95-5} is the $5-95\%$ significant bandwidth that contains 90% of the total energy. The total energy of the time series is conserved in wavelet packets because of the orthogonality of the wavelet packet function. To capture the other four time-domain parameters using wavelet packets, we employ the following parameters:

$$E(t) = \sum_i\sum_k t_k\left|c_{j,k}^i\right|^2/E_{acc} \qquad (17)$$

$$S^2(t) = \sum_i \sum_k \{t_k - E(t)\}^2 \left| c_{j,k}^i \right|^2 / E_{acc} \qquad (18)$$

$$E(f) = \sum_i \sum_k f_i \left| c_{j,k}^i \right|^2 / E_{acc} \qquad (19)$$

$$S^2(f) = \sum_i \sum_k \{f_i - E(f)\}^2 \left| c_{j,k}^i \right|^2 / E_{acc} \qquad (20)$$

where $E(t)$ is temporal centroid, $S^2(t)$ is temporal variance, $E(f)$ is spectral centroid, and $S^2(f)$ is spectral variance, and they are related to $E_{th}(t)$, t_{95-5}, $E_{th}(f)$, and f_{95-5} respectively. We define the time and frequency correlation of wavelet packets to control the time and frequency nonstationarity as follows:

$$\rho(t,f) = \frac{\sum_i \sum_k [t_k - E(t)][f_i - E(f)] \left| c_{j,k}^i \right|^2}{S(t)S(f)E_{acc}} \qquad (21)$$

Figure 2 shows that the target characteristics are estimated well with the parameters by the wavelet packets. By controlling wavelet packets, therefore, we can control the time and frequency characteristics of the time series.
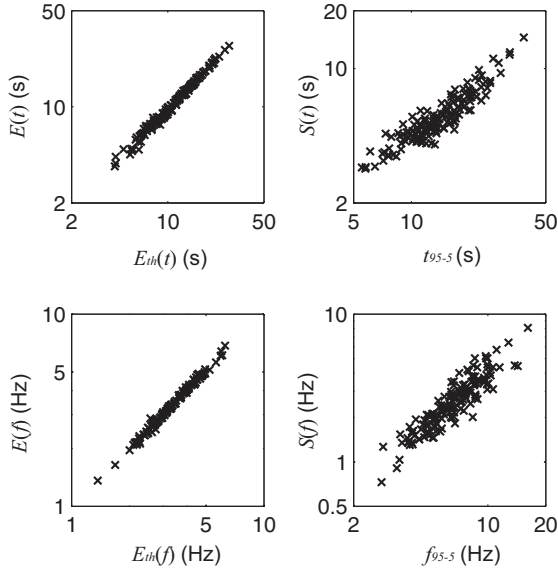

Figure 2: Comparison of parameters between from time series and wavelet packets. (a) temporal centroid, (b) $5 - 95\%$ significant duration, (c) spectral centroid, and (d) significant bandwidth.

2 STOCHASTIC MODELING OF GROUND MOTIONS USING WAVELET PACKET TRANSFORM

The proposed stochastic ground motion model employs two groups of wavelet packets (a major and minor group) because the wavelet packet transform is compressive such that only few wavelet packets have large amplitude and the others have small amplitude or zero.

The major group of wavelet packets are the largest amplitude packets that together contain 70% of the total energy in the ground motion (typically this is less than 1% of the total number of wavelet packets). The remaining smaller packets are in the minor group. The overall wavelet packets are a combination of these two groups as follows:

$$|c_{j,k}^i|^2 = |c_{j,k,maj}^i|^2 + |c_{j,k,min}^i|^2 \qquad (22)$$

where $c_{j,k,maj}^i$ and $c_{j,k,min}^i$ are the wavelet packets in the major and minor group respectively.

In the major group, the amplitudes of $|c_{j,k,maj}^i|^2$ at the time t_k and the frequency f_i are independent and identically distributed (i.i.d.) exponential random variables with $E(|c_{j,k,maj}^i|^2)$, and their time and frequency locations that are independent of the amplitudes are i.i.d. bivariate lognormal random variables with mean vector and covariance matrix of t_k and f_i.

The wavelet packets distribution in the minor group are estimated by the bivariate lognormal function of the time and frequency.

$$X_k = \ln(t_k), \ \ Y_i = \ln(f_i) \qquad (23)$$

$$|c_{j,k,min}^i|^2 = \frac{1}{2\pi S(X)S(Y)\sqrt{(1 - R(X,Y)^2)}}$$

$$\times \frac{1}{X_k Y_i} \exp \left[-\frac{A^2 - 2R(X,Y)AB + B^2}{2\{1 - R^2(X,Y)\}} \right] \times \xi_{k,i} \qquad (24)$$

$$A = \frac{X_k - E(X)}{S(X)}, \ \ B = \frac{Y_i - E(Y)}{S(Y)} \qquad (25)$$

where t_k and f_i are the time and frequency location of $c_{j,k,min}^i$, respectively, R is the correlation coefficient of $\ln(t_k)$ and $\ln(f_i)$, and $\xi_{k,i}$ are i.i.d. lognormal random variables with median one and logarithmic standard deviation of the residual of the wavelet packets in the minor group from the bivariate lognormal function.

Hence the 13 parameters are required in this model: one each of $E(t)$, $S(t)$, $E(f)$, $S(f)$, and $\rho(t,f)$ for both groups $E(|c_{j,k,maj}^i|^2)$, E_{acc} for total Energy, and the standard deviation of $\xi_{k,i}$.

There are some minor restrictions on the time and frequency boundaries of recorded ground motions, in order to avoid unreasonably long (but small amplitude) shaking in the time axis and to avoid a residual velocity. In the minor group, the stopping time of the wavelet packets given each frequency level i is the temporal centroid $+2\sigma$ given f_i of the minor group, and for in major group, the stopping time is the temporal centroid $+1\sigma$ given f_i of the minor group such that the wavelet packets in the major group suppose to exist within the main part of the ground motion. For

the frequency axis, the amplitudes of wavelet packets are zero in the lowest frequency level.

In our model, the number of the wavelet packets is 16384 and the maximum wavelet decomposition level is nine for the lowest frequency level, therefore the longest applicable period that can be modeled in the frequency domain is $10.24s$.

3   GROUND MOTION SIMULATION

Using our stochastic ground motion model, 153 ground motion recordings from the 1994 Northridge earthquake ($M_W = 6.7$) are considered. We estimated the 13 model parameters for each of these recordings. A trigger time correction is necessary when estimating the parameters because some parameters are specified relative to a time = 0 point. We define the trigger time in a recording as as the time when the absolute value of the time series crossed 1% of PGA, in order to have a consistent time = 0 point in each observation. Also, the recorded ground motions are truncated by the bandpass filters in the frequency domain to remove noise, and the filter frequencies differ ground motion to ground motion, which makes it difficult to directly estimate mean frequencies in the motions. To address this challenge, the parameters of the target ground motions are estimated by the Maximum Likelihood Method, noting the filter frequencies in the likelihood formulation.

With these estimated parameters, we then generated 300 simulations for each target and computed the median of $E_{th}(t)$, t_{95-5}, mean period (T_m Rathje et al. 2004), f_{95-5}, and $\rho(t,f)$, Arias intensity (I_a Arias 1970), spectral acceleration (S_a), and inelastic spectral displacement (S_d) from simulated ground motions.

Figures 3 and 4 show two recorded ground motions at near and far distances, respectively, and selected samples whose response spectra are the closest to the median response spectra of the simulations. For the target recordings, in the far field, PGA is smaller, $S(t)$ is larger, $\rho(t,f)$ is larger, and $S(f)$ is smaller than those in the near field. The simulations obtained from our model reflect these characteristics, which are observed empirically and expected theoretically.

In figure 5, the median of the parameters reasonably match those of target recordings except t_{95-5}. The duration t_{95-5} of the simulation tends to be longer than that of the target recording in the case of short duration because the stopping time of the recordings is unknown as well as trigger time and also the simulation doesn't stop completely in the both time and frequency axes, and the difference between the central time of adjacent wavelet packets is 2.56s. Figures 6 and 7 compare S_a and inelastic S_d, respectively, of the recordings and associated simulations, and show that the two have a reasonable match.
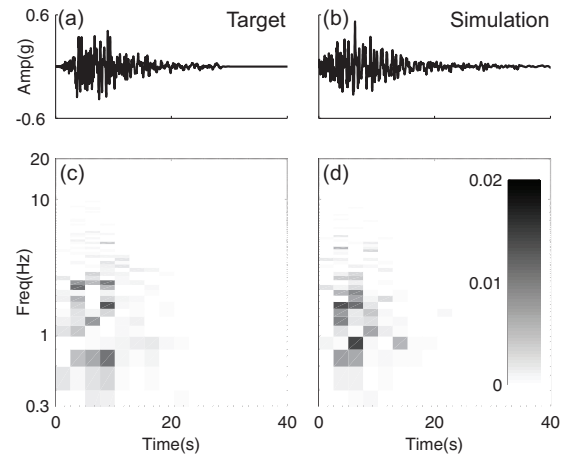

Figure 3: Recording (target) and simulation for the Northridge earthquake 17645 Saticoy St. recording ($R_{RUP} = 18km$, $V_{S30} = 281m/s$) (a),(c) time series and wavelet packets of the target recording, (b),(d) time series and wavelet packets of the simulation.
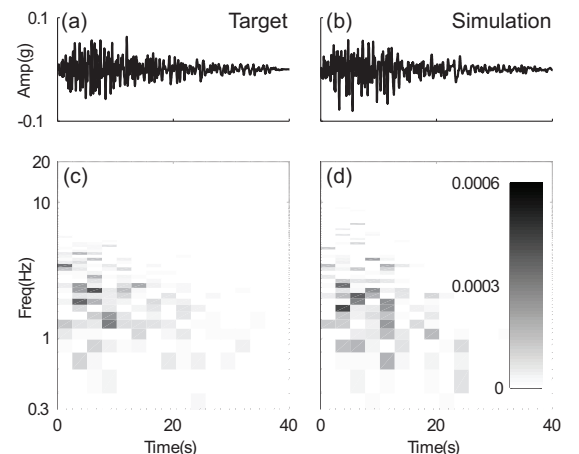

Figure 4: Recording (target) and simulation for the Northridge earthquake Santa Barbara UCSB Goleta recording ($R_{RUP} = 123km$, $V_{S30} = 339m/s$) (a),(c) time series and wavelet packets of the target recording, and (b),(d) time series and wavelet packets of the simulation.

4   REGRESSION ANALYSIS

Generating a ground motion from a particular earthquake scenario (i.e., magnitude, distance and site condition), the 13 parameters for our model need to be connected to those scenario parameters. To do this, two-stage regression analysis (Joyner and Boore 1993,1994) is employed with moment magnitude (M_W), hypocentral distance (R_{hyp}), rupture distance (R_{rup}), and average shear wave velocity within 30m depth (V_{S30}) as predictors.

The database for the regression analysis is selected from the NGA database (Chiou et al. 2008), and contains fault normal component of 1408 strong ground motion recordings from 25 earthquakes. This is a subset of the database used in the BA08 (Boore and Atkinson 2008) model. For each of these ground motions, all 13 parameters were estimated.

The following equation is a functional form for E_{acc}, and the other parameters have similar functional
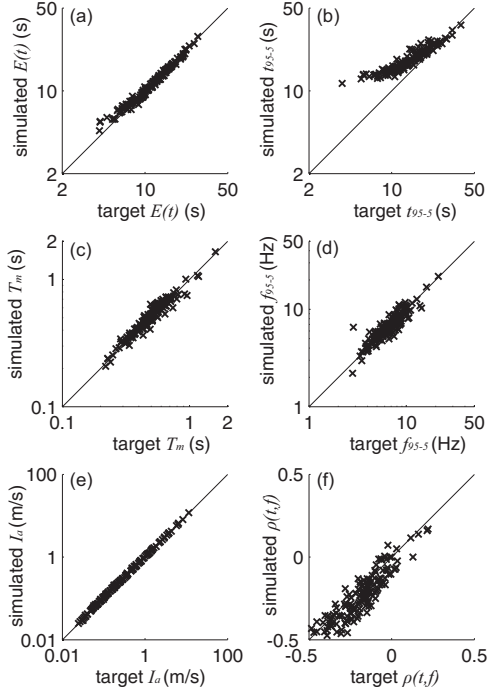
Figure 5: Model parameters between from the target time series versus the median of the corresponding parameter from 300 simulations. (a) temporal centroid, $E(t)$, (b) significant duration, t_{95-5}, (c) mean period, T_m, (d) significant bandwidth, f_{95-5}, (e) Arias intensity (I_a), and (f) correlation of wavelet packets between time and frequency, $\rho(t,f)$.

Figure 6: PGA and S_a from target time series versus median of corresponding value from simulations. (a) PGA, (b) S_a at $T = 0.2s$, (c) S_a at $T = 1s$, and (d) S_a at $T = 3s$.

Figure 7: Median of inelastic S_d with ductility $\mu = 8$ between target time series and simulations. (a) S_a at $T = 1s$, and (b) S_a at $T = 3s$.

forms:

$$\log(Y) = a + b_1 M_W + b_2 \log(M_W) + c_2 \log(R)$$
$$+ d\log(V_{S30}) + \eta + \xi \tag{26}$$

$$R = \sqrt{R_{RUP}^2 + h^2} \tag{27}$$

where η and ξ are inter-event and inter-event residuals, and these residuals for the 13 parameters are correlated each other. h is determined to minimize the mean square error of the regression analysis.

5 COMPARISON WITH GROUND MOTION PREDICTION MODELS

To evaluate the regression equations and resulting simulations, we generated 300 samples for each magnitude/distance/site condition of interest, and compare properties of the resulting simulated motions to empirical predictions of those properties from existing ground motion prediction models (GMPM). Note that for brevity, in the text below we use the abbreviations AS08, BA08, CB08, CY08 and CB10 to refer to the models of Abrahamson and Silva (2008), Boore and Atkinson (2008), Campbell and Bozorgnia (2008), Chiou and Youngs (2008) and Bozorgnia et al. (2010), respectively.

The S_a and inelastic response spectra are computed for $M_W = 7$, vertical strike-slip fault, and $V_{S30} = 270m/s$ for the Joyner-Boore distance ($1 \leq R_{JB} \leq 100km$). The Inelastic response spectra here is defined
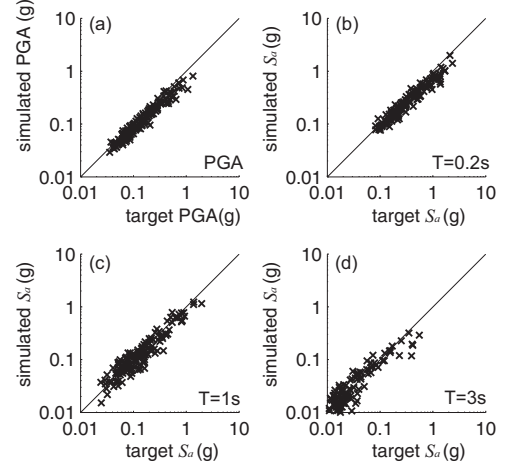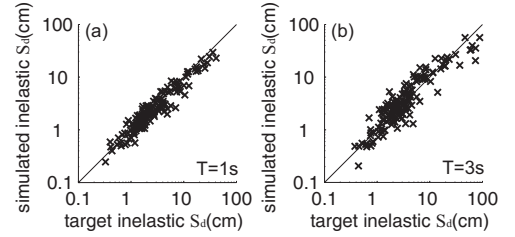
as F_y/W (where F_y is the yield strength and W is the weight of the single-degree-of-freedom system), and are computed for elastic-perfectly-plastic (EPP) systems with 5% viscous damping ratio and ductility ratio $\mu = 8$ for inelastic behavior of force and displacement (Chopra 2007).

Figures 8, 9, and 10 show the median and logarithmic standard deviation of S_a and F_y/W, for both the ground motions produced by our model and the predictions from modern empirical models for those parameters. The results from our simulations match well with those from the NGA GMPM except the case with $T = 3s$. This discrepancy occurs in part because the wavelet packets at low frequencies have low resolution in the frequency domain, and so the fluctuation of the amplitude and frequency of wavelet packets at long periods cause large variations in S_a.

The parameters t_{95-5}, mean period (T_m, Rathje et al. 2004), and Arias intensity (I_a, Arias 1970) are computed for a $M_W = 7$, vertical strike-slip fault with $V_{S30} = 270m/s$ and $1 \leq R_{RUP} \leq 100km$. Figure 11 shows the medians and logarithmic standard deviations of t_{95-5}, T_m, and I_a observed in our simulations and predicted by appropriate GMPMs. All of these parameters from our simulations reasonably match those from GMPM predictions.

Finally, prediction error ε (Baker and Cornell 2005) is computed for simulations with $M_W = 7$, $R_{RUP} = 10km$, $V_{S30} = 270m/s$. The ε of ground motion recordings are considered to be normally distributed (Jayaram and Baker 2008) and the correlation of the

ε at the different periods are correlated (Baker and Jayaram 2008). Figure 12 shows a normal quantile-quantile plot (Q-Q plot) for ε computed at $T = 1s$ (indicating normality of the simulation ε's), and the correlation of ε at pairs of periods (indicating good agreement with correlations in recorded ground motions, as reported by Baker and Cornell 2005).
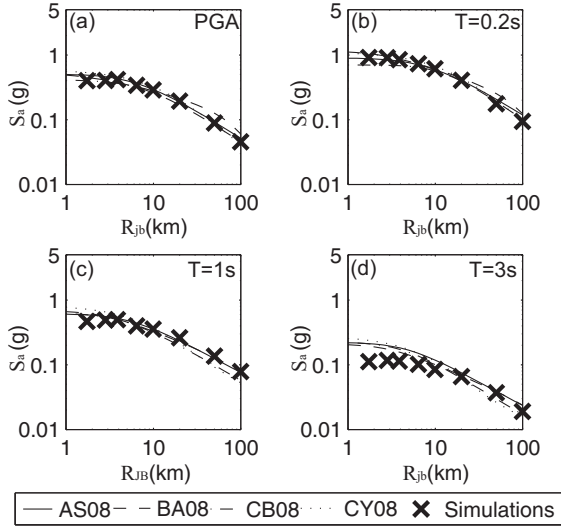

Figure 8: Median of PGA and elastic S_a computed from the NGA GMPM and simulations. (a) PGA, (b) S_a at $T = 0.2s$, (c) S_a at $T = 1s$, and (d) S_a at $T = 3s$.
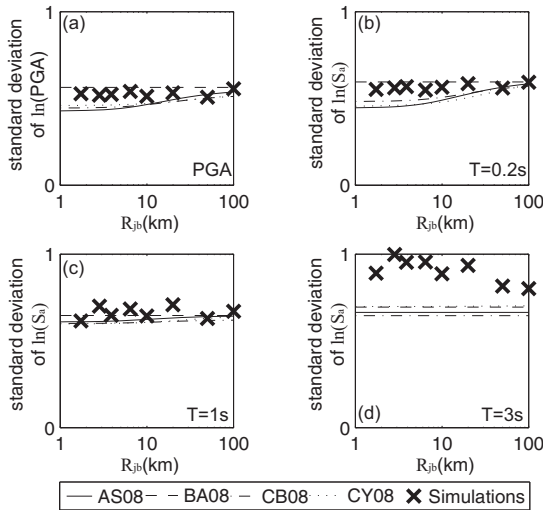

Figure 9: Logarithmic standard deviation of PGA and elastic S_a computed from the NGA GMPM and simulations. (a) *PGA*, (b) S_a at $T = 0.2s$, (c) S_a at $T = 1s$, and (d) S_a at $T = 3s$.

6 CONCLUSIONS

A stochastic model for simulating earthquake ground motions with time and frequency nonstationarity using wavelet packets has been developed. The proposed model uses wavelet packets to describe amplitude of the motion as a function of time and frequency; due to these packets having time and frequency localization, they are comparable to an evolutionary power spectral density. This model can simulate the target ground motion recordings having PGA,
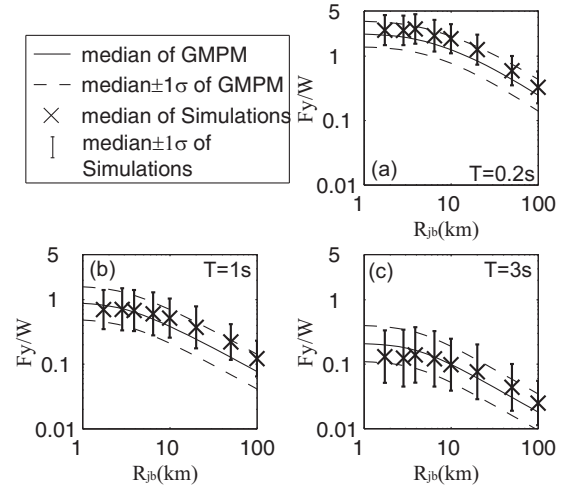

Figure 10: Median +/- σ bounds of F_y/W with ductility $\mu = 8$ computed from the GMPM and simulations. (a) S_a at $T = 0.2s$, (b) S_a at $T = 1s$, and (c) S_a at $T = 3s$.
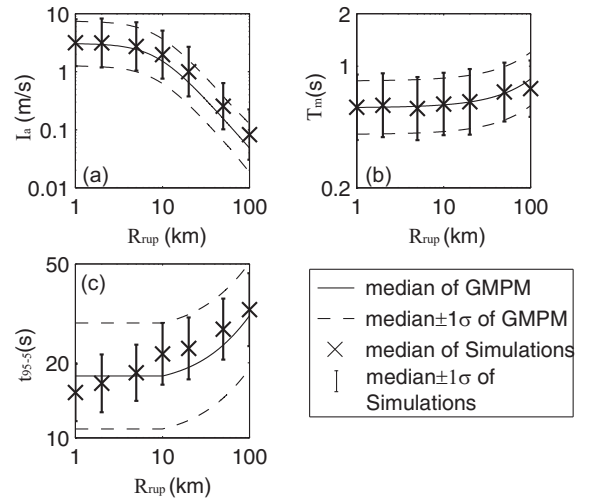

Figure 11: Median +/- σ bounds of other ground motion parameters computed from GMPMs and simulations. (a) simulated I_a and predictions from Travasarou et al. (2003), (b) simulated T_m and predictions from Rathje et al. (2004), and (c) simulated t_{95-5} and predictions from Abrahamson and Silva (1996).

significant duration, mean period, significant bandwidth, Arias intensity, and the S_a and F_y/W values that are comparable (in central value and variability) to those same properties observed in recorded ground motions. Furthermore, this model can simulate a ground motion with a specified moment magnitude, hypocentral distance, rupture distance, and V_{S30}. Additionally, the prediction errors of S_a (i.e., ε) are seen to be normally distributed and have correlation that is consistent with observations in recorded ground motions. These results suggest that the synthetic ground motions generated by the proposed model can be used for the non-linear dynamic structural analysis as the input ground motions. Current work is studying whether these simulations do in fact produce appropriate levels of response in non-linear structural models.
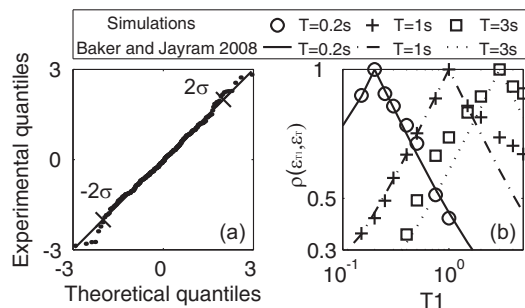
Figure 12: The characteristics of ε. (a) the Q-Q plots of the ε and (b) the correlation of the ε in different periods.

7 SOFTWARE

The stochastic model described here is implemented in the Matlab programming environment using the Matlab Wavelet Toolbox. Source code and further documentation are available at stanford.edu/~bakerjw/gm_simulation.html. The web site also contains regression coefficients, earthquake ground motion list used in regression analysis, and other relevant information for the validation of this model. The current algorithm requires 1 hour for 1000 simulations on a desktop computer (Dell Optiplex 740 with AMD Athlon 64 dual core and 2GB of RAM).

8 ACKNOWLEDGEMENT

REFERENCES

Abrahamson, N. & W. Silva (2008). Summary of the Abrahamson & Silva NGA ground-motion relations. *Earthquake Spectra 24*(1), 67.

Abrahamson, N. A. & W. J. Silva (1996). Empirical ground motion models. *Brookhaven National Laboratory*.

Arias, A. (1970). A measure of earthquake intensity. *Seismic Design for Nuclear Power Plants*, Hansen RJ (ed.). MIT Press: Cambridge, MA, 438–483.

Baker, J. W. & A. Cornell (2005). A vector-valued ground motion intensity measure consisting of spectral acceleration and epsilon. *Earthquake Engineering & Structural Dynamics 34*(10), 1193–1217.

Baker, J. W. & N. Jayaram (2008). Correlation of Spectral Acceleration Values from NGA Ground Motion Models. *Earthquake Spectra 24*(1), 299.

Bazzuro, P. & N. Luco (2006). Do scaled and spectrum-matched near-source records produce biased nonlinear structural responses? *Conference, National Engineering, Earthquake Engineering 94111*.

Boore, D. M. & G. M. Atkinson (2008). Ground-motion prediction equations for the average horizontal component of PGA, PGV, and 5%-damped PSA at spectral periods between 0.01s and 10.0s. *Earthquake Spectra 24*(1), 99.

Bozorgnia, Y., M. M. Hachem, & K. W. Campbell (2010). Ground motion prediction equation (Attenuation Relationship) for inelastic response spectra. *Earthquake Spectra 26*(1), 1.

Campbell, K. W. & Y. Bozorgnia (2008). NGA ground motion model for the geometric mean horizontal component of PGA, PGV, PGD and 5% damped linear elastic response spectra for periods ranging from 0.01s to 10s. *Earthquake Spectra 24*(1), 139.

Chakravorty, M. K. & E. H. Vanmarck (1973). Probabilistic seismic analysis of light equipment within buildings. *Proc. of 5th World Conference on Earthquake Engineering, Rome, Italy*.

Chiou, B., R. Darragh, N. Gregor, & W. Silva (2008). NGA project strong-motion database. *Earthquake Spectra 24*(1), 23.

Chiou, B. S.-J. & R. R. Youngs (2008). An NGA Model for the average horizontal component of peak ground motion and response spectra. *Earthquake Spectra 24*(1), 173.

Chopra, A. K. (2007). *Dynamics of structures*. Upper Saddle River, NJ.: Prentice Hall.

Graves, R. W. & a. Pitarka (2010). Broadband ground-motion simulation using a hybrid approach. *Bulletin of the Seismological Society of America 100*(5A), 2095–2123.

Jayaram, N. & J. W. Baker (2008). Statistical tests of the joint distribution of spectral acceleration values. *Bulletin of the Seismological Society of America 98*(5), 2231–2243.

Joyner, W. B. & D. M. Boore (1993). Methods for regression analysis of strong-motion data. *Bulletin of the Seismological Society of America 83*(2), 469–487.

Joyner, W. B. & D. M. Boore (1994). Errata. *Bulletin of the Seismological Society of America 84*(3), 955–956.

Luco, N. & P. Bazzurro (2007). Does amplitude scaling of ground motion records result in biased nonlinear structural drift responses ? *Earthquake Engineering and Structural Dynamics 36*, 1813–1835.

Meyer, Y. (1986). Principe d'incertitude, bases hilbertiennes et algebres d'operateurs. *Séminaire N. Bourbaki 662*, 209–223.

Priestley, M. B. (1996). Wavelets and time-dependent spectral analysis by m. b. priestley. *Journal of Time Series Analysis 17*(1), 85–103.

Rathje, E. M., F. Faraj, S. Russell, & J. D. Bray (2004). Empirical relationships for frequency content parameters of earthquake ground motions. *Earthquake Spectra 20*(1), 119.

Rezaeian, S. & A. D. Kiureghian (2008). A stochastic ground motion model with separable temporal and spectral nonstationarities. *Earthquake Engineering and Structural Dynamics 37*, 1565–1584.

Rezaeian, S. & A. D. Kiureghian (2010). Simulation of synthetic ground motions for specified earthquake and site characteristics. *Earthquake Engineering and Structural Dynamics 39*, 1155–1180.

Spanos, P., a. Giaralis, & N. Politis (2007). Timefrequency representation of earthquake accelerograms and inelastic structural response records using the adaptive chirplet decomposition and empirical mode decomposition. *Soil Dynamics and Earthquake Engineering 27*(7), 675–689.

Spanos, P. D. & G. Failla (2004). Evolutionary spectra estimation using wavelets. *Journal of Engineering Mechanics 130*(8), 952.

Thráinsson, H. & A. S. Kiremidjian (2002). Simulation of digital earthquake accelerograms using the inverse discrete Fourier transform. *Earthquake Engineering & Structural Dynamics 31*(12), 2023–2048.

Travasarou, T., J. D. Bray, & N. A. Abrahamson (2003). Empirical attenuation relationship for Arias Intensity. *Earthquake Engineering & Structural Dynamics 32*(7), 1133–1155.

Trifunac, M. D. & A. G. Brady (1975). A study on the duration of strong earthquake ground motion. *Bulletin of the Seismological Society of America 65*(3), 581–626.